J. Serb. Chem. Soc. 91 (0) 1–12 (2026)
JSCS–13775

Original scientific paper
Published 00 MM, 2026

Process optimization and economic calculation of photocatalytic degradation of methylene blue over sulfur-doped g-C_3N_4

WEI LI[1]* and SHUYU CAO[2]

[1]*Department of Economics, Heilongjiang University of Finance and Economics, Harbin 150025, China and* [2]*Department of Science and Technology, Heilongjiang University of Finance and Economics, Harbin 150025, China*

(Received 12 February, revised 10 April, accepted 19 May 2026)

Abstract: Sulfur doping has been considered an effective strategy to enhance the photocatalytic activity of graphitic carbon nitride (g-C_3N_4). However, there are no reports on the process optimization and economic calculation to determine the optimal photocatalytic parameters and compare the operating costs, respectively. In this work, sulfur-doped g-C_3N_4 (S/g-C_3N_4) was prepared *in situ* by a one-pot pyrolysis approach using thiourea as the precursor and sulfur source. S/g-C_3N_4 was characterized by various instrumental techniques. Response surface methodology (RSM) was employed to determine the optimal photocatalytic conditions for the degradation of Methylene blue (MB) over S/g-C_3N_4. A central composite design (CCD) with four factors at five levels was established, comprising 30 experimental runs. The optimal conditions were determined as an initial MB concentration of 27.6 mg L^{-1}, a catalyst dosage of 4.1 g L^{-1}, a solution pH of 8.7 and a reaction time of 127 min. Under these conditions, the predicted degradation efficiency could reach 99.94 %, while the experimental value was 99.5 %. Cost accounting indicated that the optimization substantially reduced direct costs, greatly improved equipment utilization, and enhanced operational flexibility. This work will lay key foundation for cost control and efficiency improvement in the scale-up application of g-C_3N_4-based photocatalysts.

Keywords: graphitic carbon nitride; photocatalyst; response surface methodology; cost accounting.

INTRODUCTION

Resource shortages and environmental pollution are closely related to our quality of life and health conditions, and have drawn considerable attention from governments around the world. Among the two, the issues caused by environmental pollution are more significant.[1] Among various kinds of environmental pollution, organic dye wastewater has attracted the most attention because of its high

* Corresponding author. E-mail: lilidezhicheng@sina.com
https://doi.org/10.2298/JSC260212027L

concentration, diverse composition, difficult decolorization, widespread pollution and complex structure. At present, there are many technologies to treat organic dye wastewater, including adsorption, membrane separation, biodegradeation, extraction, oxidation and so on.[2] In recent years, the development of advanced oxidation technologies represented by photocatalytic oxidation has attracted considerable attention. The use of photocatalytic materials to purify water has become a high-tech environmental purification technology of global concern.[3]

In recent decades, a variety of novel visible-light-response photocatalytic materials have been developed, such as bismuth oxyhalides, metal-organic frameworks, $ZnIn_2S_4$, $CuFeS_2$, WO_3, $CuWO_4$, Cu_2SnS_3 and others. These materials have high visible-light catalytic stability and activity.[4–7] However, the precious metals in the components increase the preparation and production costs of photocatalytic materials. At the same time, they have certain toxicity and the potential to pollute the water environment. Therefore, these materials are not suitable for large-scale practical applications. Graphitic carbon nitride (g-C_3N_4) is a new type of non-metallic semiconductor with a band gap of about 2.7 eV, which can achieve visible light response and make full use of solar energy. Moreover, g-C_3N_4 has a stable structure, controllable performance, a non-toxic and harmless nature, acid and alkali resistance, and light corrosion resistance. It has become a hotspot in the research field of photocatalytic materials.[8,9] However, the shortcomings of g-C_3N_4, such as fast electron-hole recombination and a small specific surface area, limit its practical application. Therefore, heterojunction construction, doping modification, microstructure regulation and other methods have been employed to improve the photocatalytic activity of g-C_3N_4.[10,11] Among them, doping with non-metallic elements could effectively change the electronic band structure of g-C_3N_4, thereby improving its photocatalytic activity.[12] Xu and coworkers successfully prepared g-C_3N_4 with nitrogen defects and sulfur doping *via* a cold plasma technique. S--doping could offer more active sites for the photocatalytic process and enhance the stability of N defects. The visible light photocatalytic activity of S-doped g--C_3N_4 was 11.25 times higher than that of pure g-C_3N_4.[13] Ma *et al.* used the dielectric barrier discharge (DBD) plasma to obtain an S-doped g-C_3N_4 photocatalyst under an H_2S atmosphere. They found that DBD plasma treatment could make more sulfur be doped into the g-C_3N_4 lattice than traditional roasting approach. The as-prepared S-doped g-C_3N_4 exhibited much higher photocatalytic degradation efficiency of rhodamine B (RhB).[14] In addition, a porous S-doped g-C_3N_4 was successfully prepared *via* one-step calcination method by Yang and coworkers. The as-prepared porous S-doped g-C_3N_4 displayed approximately 6.2 times higher peroxymonosulfate activation capacity for the degradation of RhB than pristine g-C_3N_4 under visible light irradiation.[15] Song *et al*. employed urea and thiourea as precursors to prepare S-doped g-C_3N_4 nanosheets through physical steam activation. The as-prepared photocatalyst exhibited 2.1 and 5.52 fold higher

decomposition efficiency and reaction rate for the photodegradation of Methylene blue (MB) dye than bulk g-C_3N_4, respectively.[16] Overall, S doping has been proven to be an efficient strategy to improve light absorption and photogenerated electron–hole separation, consequently boosting the photocatalytic activity of g-C_3N_4.[17] However, there are few reports on the process optimization of photocatalytic degradation of organic pollutants over S-doped g-C_3N_4. Response surface methodology (RSM) based on a central composite design (CCD) is a widely used process parameter optimization method.[18–20] This methodology includes experimental condition design and parameter optimization. The specific steps of this methodology can be divided into the following four aspects:[21,22] 1) determination of the variables and experimental design, 2) evaluation of the parameters for mathematical model regression analysis, 3) prediction of the model response and 4) confirmation of the accuracy of the model. In addition, as far as we know, the economic calculation of photocatalytic degradation of organic pollutants over S-doped g-C_3N_4 before and after process optimization has not been investigated.

Therefore, in this work, S-doped g-C_3N_4 was prepared by a facile one-pot pyrolysis approach using thiourea as the precursor and sulfur source to realize *in situ* S doping and achieve high photocatalytic activity. Based on the characterization analyses and photocatalytic performance evaluation of S-doped g-C_3N_4, the RSM method was employed for the first time to optimize the process of MB photodegradation over S-doped g-C_3N_4 to determine the optimal operating parameters. Moreover, the economic calculations before and after optimization were performed for the first time. Therefore, this work will lay an engineering and cost foundation for the large-scale practical applications of g-C_3N_4-based photocatalysts.

EXPERIMENTAL

Preparation of S-doped g-C_3N_4

A facile one-pot pyrolysis approach was employed to prepare in situ S-doped g-C_3N_4 using thiourea as the precursor and sulfur source.[23] The specific procedures are as follows: 15 g of thiourea was weighed and put into a 100 mL crucible, and then heated from room temperature to 550 °C at a heating rate of 20 °C/min in a muffle furnace. After being kept for 4 h, the sample was cooled to room temperature in the furnace. Finally, it was ground into powder for subsequent use.

Characterization techniques

X-ray diffraction (XRD), Fourier transform infrared spectroscopy (FTIR), field emission scanning electron microscopy (FESEM), transmission electron microscopy (TEM) and UV–Vis diffuse reflectance spectroscopy (UV–Vis DRS) were used to characterize the as-prepared samples. The detailed information is provided in the supplementary file.

Photocatalytic experiments

The photocatalytic performance of S-doped g-C_3N_4 was evaluated using MB dye as the target pollutant. The experimental procedure is provided in the Supplementary material to this paper.

RSM optimization method

In this work, four parameters were selected as variables, namely the initial MB concentration (mg L^{-1}), catalyst dosage (g L^{-1}), solution pH and reaction time (min), which were labeled as X_1, X_2, X_3 and X_4, respectively. At the same time, the degradation rate of MB dye was used as the output response (Y). The detailed descriptions of experimental design, mathematical modeling and response optimization are provided in the Supplementary material. In addition, the range and the level of independent variables are shown in Table S-I of the Supplementary material.

Economic calculation method

Generally, the standardized economic calculation for a wastewater treatment process included three main parts: raw material cost, operation cost and integrated cost.[24-26] Their calculation methods are provided in the Supplementary material.

RESULTS AND DISCUSSION

Characterization of S-doped g-C_3N_4

Fig. 1A presents the XRD pattern of the S-doped g-C_3N_4 sample. The XRD pattern shows two prominent diffraction peaks located at 2θ 13 and 27.5°. The peak at 13° belongs to the in-plane ordering of triazine units and is indexed to the (100) crystal plane of g-C_3N_4, whereas the peak at 27.5° corresponds to the interlayer stacking of aromatic layers and is assigned to the (002) crystal plane of g-C_3N_4.[27] The FT-IR spectrum of S-doped g-C_3N_4 is displayed in Fig. 1B. The absorption bands in the 1225–1640 cm^{-1} region are assigned to stretching vibrations of C–N and C=N bonds within the N-containing ring framework, together with exocyclic C–N stretching.[28] The broad band at 3135 cm^{-1} is associated with N–H stretching vibrations,[29] while the band at 796 cm^{-1} is attributed to the bending vibration of the C–N ring.[30]

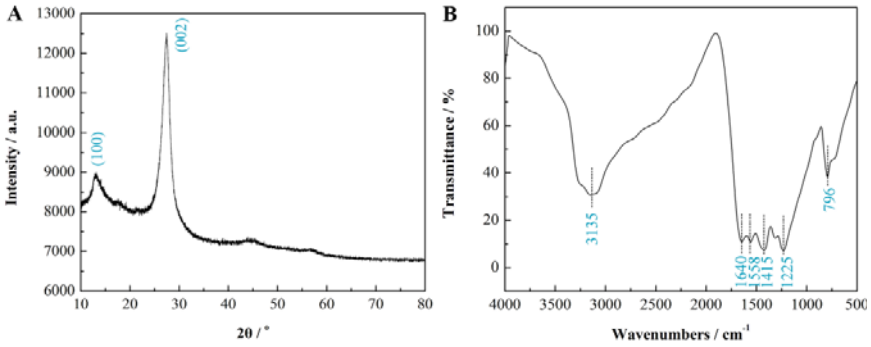

Fig. 1. A) XRD pattern and B) FTIR spectrum of S-doped g-C_3N_4.

Fig. 2A gives an FESEM image of S-doped g-C_3N_4, displaying a non-uniform particulate morphology in which the particles are irregularly agglomerated, consistent with the typical morphology of g-C_3N_4.[31] Fig. 2B shows a TEM image of the

S-doped g-C_3N_4 sample. It can be seen that the as-prepared sample has a typical thin-layer structure with some wrinkles, similar to graphene. This thin-layer structure will further increase the specific surface area of the S-doped g-C_3N_4 sample, thereby improving the adsorption capacity and photocatalytic activity of the sample.[32] From the energy-dispersive spectrum (EDS) of S-doped g-C_3N_4 (Fig. 2C), it can be clearly seen that the as-prepared sample contains three main elements C, N and S, which indicates that S has been successfully introduced into g-C_3N_4. In addition, no characteristic diffraction peak or absorption peak belonging to S was found in the XRD pattern and the FTIR spectrum, which implies that S might enter the crystal structure of g-C_3N_4 and replace C or N, rather than as impurities.[13–16]

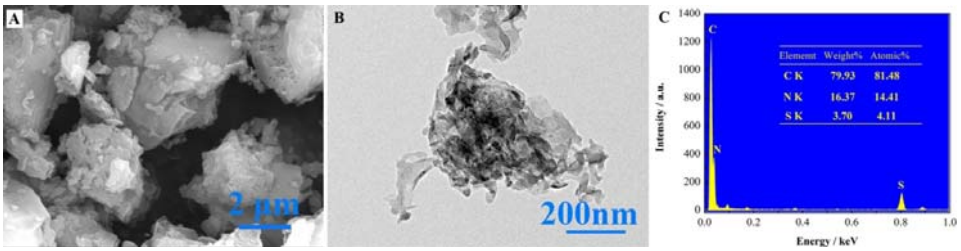

Fig. 2. A) FESEM, B) TEM and C) EDS images of S-doped g-C_3N_4.

Fig. 3A shows the UV–Vis DRS spectrum of S-doped g-C_3N_4, from which it can be observed that the S-doped g-C_3N_4 sample has strong visible-light absorption and an absorption edge is located at approximately 412 nm. According to the extrapolation of $(F(R)–h\nu)^{1/2}$ curve *vs.* photon energy $h\nu$ (Fig. 3B), the band gap (E_g) of S-doped g-C_3N_4 is estimated to be 2.63 eV, in agreement with literature reports.[33] Notably, the as-prepared sample exhibits an additional absorption feature near 645 nm in the UV–Vis DRS spectrum, corresponding to an E_g of 1.81 eV. This might be associated with an S-induced impurity energy level in the band structure,[34] which can facilitate the enhancement of photocatalytic performance.

Process optimization of MB photodegradation over S-doped g-C_3N_4

To evaluate the photocatalytic performance of S-doped g-C_3N_4, MB with analytical purity was used as the target pollutant under the conditions of 10 mg L^{-1} MB, 5.0 g L^{-1} S-doped g-C_3N_4, pH 7 and room temperature. As shown in Fig. 4A, after 60 min in the dark to reach adsorption equilibrium, the removal rate of MB is only 9.4 %, suggesting that the contribution of adsorption to MB removal can be neglected. However, after 120 min of photocatalytic irradiation, the corresponding degradation rate increased to 95.8 %. Accordingly, the as-prepared S-doped g-C_3N_4 sample exhibits stronger photocatalytic performance toward MB degradation. Additionally, this photocatalytic process follows the pseudo-first-order kinetic model (Fig. 4B), with a reaction rate constant of 0.02296 min^{-1}. The UV–Vis absorption spectra of the MB solution during different photocatalytic periods are

presented in Fig. 4C, where it can be seen that the main absorption peak of the MB dye molecule at 650 nm disappeared after 120 min of photocatalytic reaction, indicating that the dye molecule has been decomposed. In addition, the removal percentage of total organic carbon (TOC) after 120 min of photocatalytic irradiation was measured as 78.4 %. Therefore, it can be supposed that the MB dye was decomposed into CO_2, H_2O, and other low-molecular-weight substances.

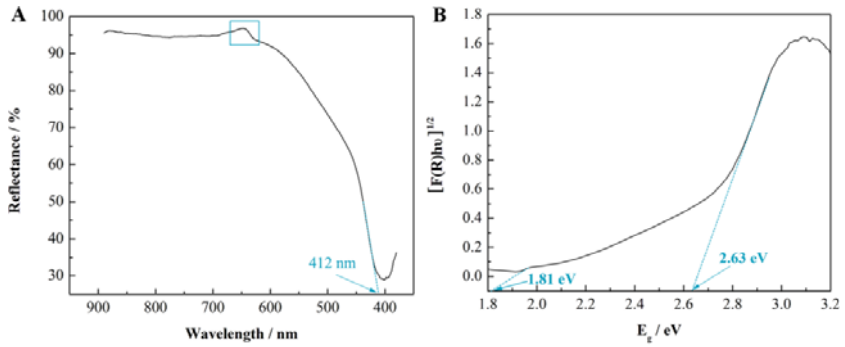

Fig. 3. A) UV–Vis DRS spectrum and B) $(F(R)–h\nu)^{1/2}$ *versus* $h\nu$ curve of S-doped g-C_3N_4.

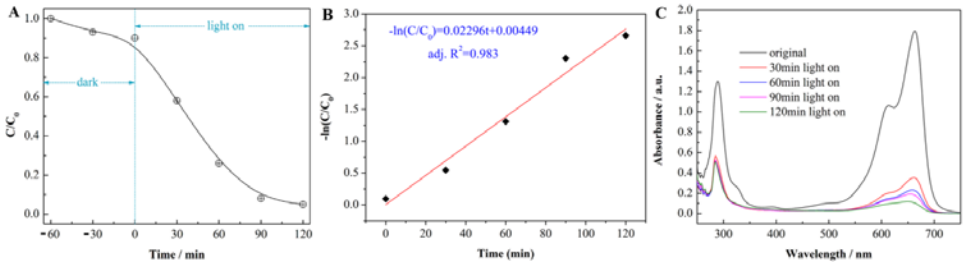

Fig. 4. A) Photocatalytic performance toward MB degradation over S-doped g-C_3N_4; B) fitting line of the pseudo-first-order kinetic model; C) UV–Vis absorption spectra of the MB solution during different photocatalytic periods.

Based on the above results, the effects of different experimental parameters on the degradation rate of MB dye were evaluated by RSM. According to the CCD, an experimental scheme with 4 factors and 5 levels was designed, and a total of 30 sets of experiments were carried out. The CCD experimental matrix is listed in Table S-II of the Supplementary material, along with the experimental and predicted values of the response *Y*. Among them, six groups of experiments are replicate experiments at the center point, which ensures that the relative error of the experiment is small. Their close response values mean higher experimental accuracy.[35]

To predict the response value, the experimental values were fitted by a second-order polynomial regression model, and the results are shown as:

$$Y = 66.46 + 5.82X_1 - 13.35X_2 + 7.62X_3 + 12.70X_4 - 2.74X_1X_2 + \\ +1.69X_1X_3 + 1.70X_1X_4 + 0.79X_2X_3 + 0.21X_2X_4 - 1.17X_3X_4 - \\ -2.48X_1^2 - 3.90X_2^2 - 10.22X_3^2 - 2.61X_4^2 \quad (1)$$

From the analysis of variance (ANOVA, Table S-III of the Supplementary material), it can be seen that the F value is 8.09, which is much higher than the standard value $F_{0.05} = 2.42$, which means that the second-order polynomial model is highly significant. In addition, as listed in Table S-II, the experimental and predicted values of the response Y are relatively close, with a correlation coefficient of $R^2 = 0.9588$. This is the main criterion for evaluating the correlation between the experimental and predicted values.[36]

Moreover, the predicted response values are in good agreement with the experimental values (Fig. S-2 of the Supplementary material). Furthermore, the *Prob* > *F* value is less than 0.0500, which means that the influence of the variable is significant, whereas the value greater than 0.1000, indicates that the influence of the variable is not significant.[37] Therefore, in this work, it can be seen from Table S-III that X_1, X_2, X_3, X_4, X_1X_3, X_1X_4, X_1^2, X_3^2 and X_4^2 are the significant influencing variables during the MB photodegradation over S-doped g-C_3N_4. In addition, the statistical analysis of the experimental data indicates that the initial MB dye concentration, S-doped g-C_3N_4 dosage, solution pH and reaction time have significant effects on MB photodegradation.

The three-dimensional (3D) response surface plots of the interaction effect between two factors are shown in Fig. 5, including the interactions between initial MB concentration and S-doped g-C_3N_4 dosage, initial MB concentration and solution pH, initial MB concentration and reaction time, S-doped g-C_3N_4 dosage and solution pH, S-doped g-C_3N_4 dosage and reaction time and solution pH and reaction time. It can be seen that the degradation rate of MB increases with the decrease in the initial MB concentration and the increase in the S-doped g-C_3N_4 dosage (Fig. 5A); increases with the decrease in the initial MB concentration and the increase in the solution pH (Fig. 5B); increases with the decrease in the initial MB concentration and the increase of the reaction time (Fig. 5C); increases with the increase of the S-doped g-C_3N_4 dosage and the solution pH (Fig. 5D); increases with the increase in the S-doped g-C_3N_4 dosage and the reaction time (Fig. 5E); increases with the increase in the reaction time and the solution pH (Fig. 5F). According to the prediction model, the process parameters of MB photodegradation over the S-doped g-C_3N_4 photocatalyst are optimized as follows: the initial MB concentration is 27.6 mg L^{-1}, the S-doped g-C_3N_4 dosage is 4.1 g L^{-1}, the solution pH is 8.7, and the reaction time is 127 min. Under these optimal conditions, the predicted degradation rate of MB can reach 99.94 %. Under the identical conditions, the experimental value of the MB degradation rate is 99.5 %, showing excellent agreement with the model prediction.

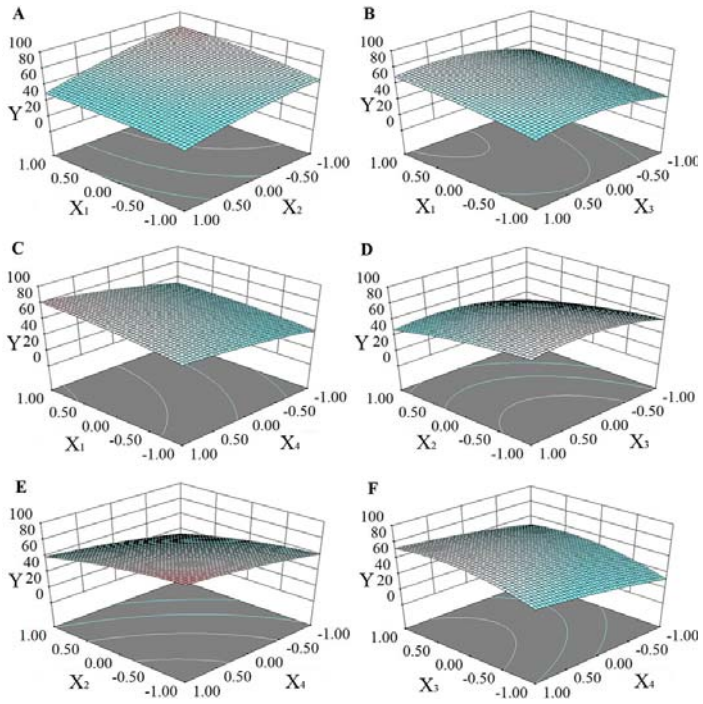

Fig. 5. 3D response surface of MB photodegradation (Y) over S-doped g-C_3N_4 with the interaction effect between: A) initial MB concentration (X_1) and S-doped g-C_3N_4 dosage (X_2), B) initial MB concentration (X_1) and solution pH (X_3), C) initial MB concentration (X_1) and reaction time (X_4), D) S-doped g-C_3N_4 dosage (X_2) and solution pH (X_3), E) S-doped g-C_3N_4 dosage (X_2) and reaction time (X_4) and F) solution pH (X_3) and reaction time (X_4).

Economic calculation of MB photodegradation over S-doped g-C_3N_4

1) Comparative analysis of raw material cost. Table S-IV of the Supplementary material provides the comparative analysis of raw material cost before and after optimization. Before optimization, the catalyst cost for treating 1 m^3 of MB wastewater was 5 kg×80 CNY kg^{-1} = 400 CNY. After optimization, the corresponding cost for treating 1 m^3 of MB wastewater was 4.1 kg×80 CNY kg^{-1} = 328 CNY. Therefore, the catalyst cost for treating 1 m^3 wastewater was reduced by 72 CNY, with a decrease of 17.8 %. Moreover, after optimization, the pH value of MB solution was adjusted from 7.0 to 8.7, so sodium hydroxide needed to be added to adjust the pH value. Based on the calculation of the acid-base balance, 0.12 kg of sodium hydroxide was required to adjust the pH from 7.0 to 8.7 for 1 m^3 wastewater, and the corresponding cost was 0.12 kg×2.5 CNY kg^{-1} = 0.3 CNY. After optimization, although the acid-base adjustment cost was slightly increased, combined with the significant reduction in catalyst cost, the integrated raw material

cost still achieved a net saving of 71.7 CNY for treating 1 m^3 wastewater, with a reduction of 17.7 %.

2) Comparative analysis of operation cost. Table S-V of the Supplementary material gives the comparative analysis of operation cost before and after optimization. The energy consumption of photocatalytic reaction mainly came from the xenon lamp (300 W) and the stirrer (50 W). The energy consumption was positively correlated with the reaction time. Before optimization, the energy consumption for treating 1 m^3 wastewater was (300 W + 50 W)×3 h = 1.05 kWh and the corresponding energy cost was 1.05 kWh×0.6 CNY kWh^{-1} = 0.63 CNY. After optimization, the reaction time was 127 min (2.12 h). Therefore, the energy consumption for treating 1 m^3 wastewater was (300 W + 50 W)×2.12 h = 0.742 kWh, and the corresponding energy cost was 0.742 kWh×0.6 CNY kWh^{-1} = 0.445 CNY. Therefore, after optimization, the energy consumption cost for treating 1 m^3 wastewater was reduced by 0.185 CNY, with a decrease of 29.4 %.

With regard to the labor cost, before optimization, assuming that the operation time of a single batch treatment of 1 m^3 wastewater was about 3.5 h, the labor cost was 3.5 h×30 CNY h^{-1} = 105 CNY. After optimization, the operation time was shortened to 2.5 h, and the labor cost was 2.5 h×30 CNY h^{-1} = 75 CNY. Therefore, the labor cost for treating 1 m^3 wastewater was directly reduced by 30 CNY, with a decrease of 28.6 %.

3) Comparative analysis of integrated cost. Based on the raw material and operation costs, the integrated cost for treating 1 m^3 MB wastewater was calculated. Before optimization, the integrated cost for treating 1 m^3 MB wastewater was (400 + 0 + 0.63 + 105) CNY= 505.63 CNY. After optimization, the integrated cost for treating 1 m^3 MB wastewater was (328 + 0.3 + 0.445 + 75) CNY = 403.745 CNY. Therefore, after optimization, the integrated cost for treating 1 m^3 MB wastewater was reduced by 101.885 CNY, with a decrease of 20.0 %.

CONCLUSION

In this work, S-doped g-C_3N_4 was successfully prepared by a facile one-step pyrolysis approach, using thiourea as the precursor and sulfur source. The as-prepared sample was characterized by XRD, FTIR, FESEM, TEM, EDS and UV–Vis DRS. The sample exhibited a wide visible-light absorption region, and its E_g was estimated to be 2.63 eV. Furthermore, an additional absorption feature near 645 nm was observed in the UV–Vis DRS spectrum, corresponding to an E_g of 1.81 eV. This might be associated with an S-induced impurity energy level in the band structure. The as-prepared sample exhibited stronger photocatalytic performance toward MB degradation. After 120 min of photocatalytic irradiation, the MB degradation rate reached 95.8 %. Based on RSM under CCD, the process optimization of MB photodegradation over the S-doped g-C_3N_4 photocatalyst was

conducted. Based on the economic cost calculations, after optimization, the integrated cost for the photodegradation of 1 m^3 MB wastewater over S-doped g-C_3N_4 was reduced from 505.63 to 403.745 CNY, with a decrease of 20.0 %.

SUPPLEMENTARY MATERIAL

Additional data and information are available electronically at the pages of journal website: https://www.shd-pub.org.rs/index.php/JSCS/article/view/13775, or from the corresponding author on request.

| ®úÇí

¹–Ö1œ1æ—¼1‰– –°1¼Œó—1Œł1ß1œół1 –°1°—¬öß Ê1Ö1ł—Ö—ø1Ö1¬łŒ
ØŒŁ°—Ø—¼1‰Eœ ŒÖ1øŒßół1Ł–ø—ª1Ł,ł1°1Ë «Œ" Œœ g-C_3N_4Ø1–1°—ß1Ł
óöœ –1°1œ

WEILI[1] | SHUYU CAO[2]

[1]Cdo'qsl dmsneEbnmnl hbr+H dhkmmgih'mg Umhudqphsx neEhm'mbd 'mc Ebnmnl hbr+H 'qahm 14//24+Cghm' |
[2]Cdo'qsl dmsneSkhdmbd 'mc Sdbgmnkngx+H dhkmmgih'mg Umhudqphsx neEhm'mbd 'mc Ebnmnl hbr+H 'qahm 14//24+Cghm'

ØÇñ|ð½" Ð ÅÙýñÇðÇý Åý½µð½ÅÐ ÐÈ|þ½ÅÁÇý Åµð½µÐé|Ýý ®½ñÇÕÇ,Ú½" Ð È ÇµÇþ½µ½Ã|-µ|ÑþÐ ½þµ|úÁÇÅµ| éð½È|µÁÇé Á|µð|í½ Ùé,ÐÁ|þ½ (g-C_3N_4).œ Ð›Ùµ|ý+Ù Ã|µÐð½µÙð| Á|ÅÙ ñð|ÅÙµÁ| |®úÐÚµ½˜| Ç Çñµ|ý|®½ó|˜| ÇúÇé ñðÇõÐÅ½+þ½Ç Á| Ç ÐþÇÁÇý ÅþÇý ñðÇð½ÑÙÁÙ ñð| ÇíðÐ›|ú½" Ù Çñµ|ý½ÃÁ|Š È ÇµÇþ½µ½Ã|µ|Ñþ|Š ñ½ð½ýÐµ½ð½. ö ÇúÇý ð½íÙ+g-C_3N_4 íÇñ|ð½Á ÅÙýñÇðÇý (S/g-C_3N_4) ñð|ñðÐý,ÐÁ Ð hm rhst ýÐµÇíÇý ñ|ðÇÃ|®Ð Ù ÐíÁÇý þÇð½þÙ+Ù® þÇð|-Ú»Ð" Ð µ|ÇÙðÐÐ þ½Ç ñðÐþÙðÅÇð½ | |®úÇð½ÅÙýñÇð½.ö ð½íÙ Ð |®úðÚ ÐÁ½þ½ð½þµÐð|®½ó|˜½ S/g-C_3N_4ð½®Ã|Ñ|µ|ý |ÁÅµðÙýÐÁµ½ÃÁ|ý µÐŠÁ|þ½ý½.æ½Çíðð›|ú½" ÐÇñµ|ý½ÃÁ|Š È ÇµÇþ½µ½-Ã|µ|Ñþ|Š ÙÅÃÇú½®½íÐéð½í½ó|Ù ýÐµ|ÃÐÁÅþÇé ñÃ½úÇé (M B) þÇð|Ú»Ð" Ðý S/g-C_3N_4 þÇð|Ú-»ÐÁ½ Ð ýÐµÇí½Çí®|úÁÐ ñÇúðÚ |ÁÐ (RSM).öÅñÇÅµ½ú,ÐÁ Ð í|®½Ã ÐþÅñÐð|ýÐÁµ½Å½ÑÐµ|ð|È½þµÇð½ Á½ ñÐµÁ|úÇ½+þÇ˜| Ð ÇÕÙŠú½µ|Ç 3/ ÐþÅñÐð|ýÐÁµ½ÃÁ|Š ñÇÁ½ú,½" ½.ØÇÕ| ÐÁ| ÅÙ ÅÃÐíÐ»| Çñµ|ý½ÃÁ| ÙÅÃÇú|:ñÇÑÐµÁ½þÇÃõÐÁµð½ó|˜½MB Çí27+61gL-Ý+íÇ®½þ½µ½Ã|®½µÇð½ 4+1gL-Ý+oH ð½Åµúçð½8+7 | úðÐýÐ ðÐ½þõ|Ð124 lhm.–Çí Çú|ý ÙÅÃÇú|ý½+ñðÐíú|›ÐÁ½ ÐÈ|þ½ÅÁÇÅµíÐéð½í½ó|Ð íÇÅµ|îÐ99+94 % +íÇþ ÐÐþÅñÐð|ýÐÁµ½ÃÁ½úðÐíÁÇÅµ|®ÁÇÅ|Ã½99+4 % .—Á½Ã|®½µðÇÚ þÇú½ñÇþ½®½Ã½Ð í½Çñµ|ý|®½ó|˜½®Á½Ñ½ÃÇ Åý½"ÙÐ í|ðÐþµÁÐ µðÇÚ þÇúÐ+Ù úÐÃ|þÇ˜ýÐð| ñÇÕÇ,Ú½ú½ |ÅþÇð|Ú»ÐÁÇÅµ ÇñðÐý Ð | ñÇúÐ»½ú½ ÇñÐð½µ|úÁÙ È ÃÐþÅ|Õ|Ã-ÁÇÅµ.¹ú½˜ð½í ñÇÅµ½ú,½þ,ÙÑÁÙ ÇÅÁÇúÙ ®½þÇÁµðÇÃÙ µðÇÚ þÇú½ | ñÇúÐ»½" Ð ÐÈ |þ½ÅÁÇÅµ| ñð|ñð|ýÐÁ| È ÇµÇþ½µ½Ã|®½µÇð½Á½Õ½®| g-C_3N_4Ù |ÁíÙÅµð|Åþ|ý ð½®ýÐð½ý½.

(–ð|ý,ÐÁÇ12.È ÐÕðÙ½ð½+ðÐú|í|ð½ÁÇ1/.½ñð|Ã½+ñð|Šú½»ÐÁÇ19.ý½½2/26)

REFERENCES

1. X. Z. Tang, Y. M. Xin, R. H. Chen, X. F. Ren, L. G. Gao, H. Xu, P. X. Yang, A. M. Liu, *J. Mater. Chem., A* **13** (2025) 34122-34148 (https://doi.org/10.1039/d5ta04748j)
2. G. Kavitha, M. Govindhan, S. Premkumar, *J. Water Process Eng.* **80** (2025) 109071 (https://doi.org/10.1016/j.jwpe.2025.109071)
3. M. S. N. Awang, B. L. Phoon, W. M. A. W. Daud, S. Boonyuen, J. C. Juan, *Mater. Sci. Eng., B* **324** (2026) 119025 (https://doi.org/10.1016/j.mseb.2025.119025)
4. X. S. Wang, Z. Y. Yuan, *Coord. Chem. Rev.* **548** (2026) 217184 (https://doi.org/10.1016/j.ccr.2025.217184)

5. M. Q. Xiao, J. J. Kong, W. J. Wang, B. Yang, S. Q. Guo, *J. Alloys Compd.* **1046** (2025) 184670 (https://doi.org/10.1016/j.jallcom.2025.184670)
6. J. Avinash, G. Madhumitha, S. M. Roopan, *J. Environ. Chem. Eng.* **13** (2025) 118368 (https://doi.org/10.1016/j.jece.2025.118368)
7. M. W. Xu, Y. J. Wu, X. Z. Zhao, J. Wang, G. C. Jiang, S. Li, Z. Q. Li, *J. Alloys Compd.* **1042** (2025) 184188 (https://doi.org/10.1016/j.jallcom.2025.184188)
8. M. G. Sahini, A. Parmain, I. Onoka, S. F. Mwanga, *J. Alloys Compd.* **1044** (2025) 183642 (https://doi.org/10.1016/j.jallcom.2025.183642)
9. N. Farooq, N. Qureshi, S. Hussain, A. M. Qureshi, Z. Sattar, R. K. Manavalan, N. Ullah, M. K. Aslam, *Int. J. Hydrogen Energy* **180** (2025) 151763 (https://doi.org/10.1016/j.ijhydene.2025.151763)
10. H. Noreen, A. Farooq, S. Naz, N. Amjed, A. Ahmad, A. Aftab, S. Muzammal, *J. Iran. Chem. Soc.* **22** (2025) 1659 (https://doi.org/10.1007/s13738-025-03252-6)
11. M. Zheng, M. R. Guo, F. Ma, W. W. Li, Y. J. Shao, *Nanoscale Adv.* **7** (2025) 4780 (https://doi.org/10.1039/d5na00439j)
12. C. Wen, Z. W. Xie, X. X. Gao, L. Q. Feng, Z. H. Li, P. C. Li, A. L. Wang, J. Wang, W. Q. Yao, *Colloids Surfaces, A* **727** (2025) 138402 (https://doi.org/10.1016/j.colsurfa.2025.138402)
13. H. L. Xu, X. F. Peng, J. X. Zheng, Z. Wang, *Front. Chem. Sci. Eng.* **17** (2023) 93 (https://doi.org/10.1007/s11705-022-2175-x)
14. L. Ma, S. Z. Hu, P. Li, Q. Wang, H. F. Ma, W. Li, *J. Phys. Chem. Solids* **118** (2018) 166 (https://doi.org/10.1016/j.jpcs.2018.03.017)
15. D. Yang, L. Zhao, X. T. Feng, L. L. Ma, H. M. Ding, *Funct. Mater. Lett.* **14** (2021) 2151019 (https://doi.org/10.1142/S179360472151019X)
16. W. L. Song, N. N. Zhang, X. J. Ma, X. T. Liu, D. N. Li, J. Li, *Chemistryselect* **9** (2024) e202400279 (https://doi.org/10.1002/slct.202400279)
17. M. X. Zuo, X. Y. Li, Y. S. Liang, F. X. Zhao, H. B. Sun, C. Liu, X. M. Gong, P. F. Qin, H. Wang, Z. B. Wu, L. Luo, *Sep. Purif. Technol.* **308** (2023) 122875 (https://doi.org/10.1016/j.seppur.2022.122875)
18. D. M. Azar, A. Feizbakhsh, H. A. Panahi, A. Niazi, *Int. J. Environ. Anal. Chem.* **102** (2022) 8490 (https://doi.org/10.1080/03067319.2020.1853114)
19. C. Y. Chen, Z. F. Luo, H. X. Tu, X. J. Lin, Y. W. Pang, J. F. Huang, J. Zhang, X. J. Wang, Q. Y. Cai, Z. B. Wei, J. Zeng, J. Qiu, *J. Hazard. Mater.* **486** (2025) 136986 (https://doi.org/10.1016/j.jhazmat.2024.136986)
20. H. M. Samuel, C. A. Mecha, M. M. M'Arimi, *React. Kin. Mech. Catal.* **137** (2024) 2415 (https://doi.org/10.1007/s11144-024-02650-w)
21. N. Szpisjak-Gulyás, A. N. Al-Tayawi, Z. H. Horváth, Z. Lászlo, S. Kertész, C. Hodúr, *Acta Aliment.* **52** (2023) 521 (https://doi.org/10.1556/066.2023.00235)
22. C. E. Aristizabal-Alzate, E. Castillejos-López, A. B. Dongil, M. Romero-Sáez, *Chemistryopen* **14** (2025) 202400148 (https://doi.org/10.1002/open.202400148)
23. H. Zhao, L. C. Wu, H. Y. Xu, *Sci. Adv. Mater.* **8** (2016) 1408 (https://doi.org/10.1166/sam.2016.2731)
24. M, Budych-Gorzna, L. Jaroszynski, P. Oleskowicz-Popiel, *J. Environ. Chem. Eng.* **9** (2021) 106366 (https://doi.org/10.1016/j.jece.2021.106366)
25. M. Yao, Z. Ju, Z. Ran, T. Chen, H. Pan, *J. Water Process Eng.* **69** (2025) 106626 (https://doi.org/10.1016/j.jwpe.2024.106626)
26. K. Wu, S. Y. Li, F. Jiang, J. Wang, G. L. Liu, G. H. Chen, *Water Sci. Technol.* **68** (2013) 530-536 (https://doi.org/10.2166/wst.2013.247)

27. J. Yang, X. Zhang, C. Xie, Ji. Long, Y. Wang, L. Wei, X. Yang, *J. Electron. Mater.* **50** (2021) 1067 (https://doi.org/10.1007/s11664-020-08654-1)
28. Q. H. Shen, C. Y. Wu, Z. Y. You, F. L. Huang, J. S. Sheng, F. Zhang, D. Cheng, H. Yang, *J. Mater. Res.* **35** (2020) 2148 (https://doi.org/10.1557/jmr.2020.182)
29. G. Nabi, N. Malik, W. Raza, *Inorg. Chem. Commun.* **119** (2020) 108050 (https://doi.org/10.1016/j.inoche.2020.108050)
30. S. Challagulla, S. Payra, C. Chakraborty, S. Roy, *Phys. Chem. Chem. Phys.* **21** (2019) 3174 (https://doi.org/10.1039/C8CP06855K)
31. Y. C. Ren, T. Gong, S. L. Tan, M. Chen, F. Zhou, Y. Lin, L. Yang, Q. Peng, *J. Alloys Compd.* **902** (2022) 163752 (https://doi.org/10.1016/j.jallcom.2022.163752)
32. L. F. Wang, Z. Y. Fan, X. X. Cao, P. F. Fan, Y. Xie, Q. Sun, J. S. Zhao, *Nanomaterials* **12** (2022) 2569 (https://doi.org/10.3390/nano12152569)
33. A. M. Li, X. H. Cong, H. T. Qin, W. C. Xu, X. H. Zhang, W. Z. Wang, F. Guo, *New J. Chem.* **47** (2023) 3910 (https://doi.org/10.1039/D2NJ06154F)
34. L. Dong, H. W. Chu, S. P. Xu, Y. Li, S. Z. Zhao, D. C. Li, *Nanophotonics* **11** (2022) 139 (https://doi.org/10.1515/nanoph-2021-0549)
35. B. Hernández, C.G. Blázquez, V. Aristizábal-Marulanda, M. Martín, *Ind. Eng. Chem. Res.* **59** (2020) 16720 (https://doi.org/10.1021/acs.iecr.0c03336)
36. D. H. Zhang, J. W. Liu, H. Wang, Y. Y. Wang, *Environ. Res.* **290** (2026) 123449 (https://doi.org/10.1016/j.envres.2025.123449)
37. K.-J. Wang, P.-S. Wang, *J. Water Process Eng.* **78** (2025) 108703 (https://doi.org/10.1016/j.jwpe.2025.108703).

Journal of the Serbian Chemical Society
JSCS-info@shd.org.rs • www.shd.org.rs/JSCS
J. Serb. Chem. Soc. 91 (0) S1–S6 (2026) *Supplementary material*

SUPPLEMENTARY MATERIAL TO

Process optimization and economic calculation of photocatalytic degradation of methylene blue over sulfur-doped g-C_3N_4

WEI LI[1]* and SHUYU CAO

[1]Department of Economics, Heilongjiang University of Finance and Economics, Harbin 150025, China and [2]Department of Science and Technology, Heilongjiang University of Finance and Economics, Harbin 150025, China

J. Serb. Chem. Soc. 91 (0) (2026) 000–000

EXPERIMENTAL

Characterization techniques

The crystal phase composition of the product was determined by X-ray diffraction (XRD), conducted on a Rigaku D/max-3B X-ray diffractometer (Japan). The functional groups of the sample were analyzed by Fourier transform infrared spectroscopy (FTIR), operated on a Nicolet Nexus infrared spectrometer (United States). The microscopic morphology of the sample was observed by field emission scanning electron microscopy (FESEM), realized on a FEISirion 200 scanning electron microscope (Netherlands). The microstructure of the sample was observed by transmission electron microscopy (TEM), obtained on a JEOL JEM-2010 transmission electron microscope (Netherlands). The optical absorption edge and band gap of S-doped g-C_3N_4 were analyzed by UV-vis diffuse reflectance spectroscopy (UV-vis DRS), recorded on an Ocean Optics USB4000 UV-visible diffuse reflectance spectrometer with integrating sphere, using a South African optical standard template was used as the reference. The content of total organic carbon (TOC) was measured by a XPERT-TOC/TNb TOC analyzer (Netherlands).

Photocatalytic experiments

The photocatalytic performance of S-doped g-C_3N_4 was evaluated under a 300W xenon lamp (100 mW/m^2), using MB dye as the target pollutant. The experimental procedures are as follows: 10 mg L^{-1} MB dye solution was prepared, and the absorbance of the standard solution was measured by a 722-type spectrophotometer, marked as A_0. 100 mL MB working solution was put into a 250 mL glass breaker. Then, a certain amount of S-doped g-C_3N_4 sample was added to this solution. After being stirred for 60 min, the adsorption equilibrium of the dye was obtained, and then the lamp was turned on. The schematic diagram of photocatalytic reactor is displayed in Fig. S1. During the photocatalytic reaction, about 5 mL of suspension was extracted at a specific reaction time. The supernatant was centrifuged and separated. The absorbance of the supernatant was measured and marked as A_i. The MB degradation rate was calculated by the following equation: $Y(\%) = 100(A_0-A_i)/A_0$. Meanwhile, under identical experimental conditions, random experiments were carried out to verify the repeatability of the experimental results.

* Corresponding author. E-mail: lilidezhicheng@sina.com

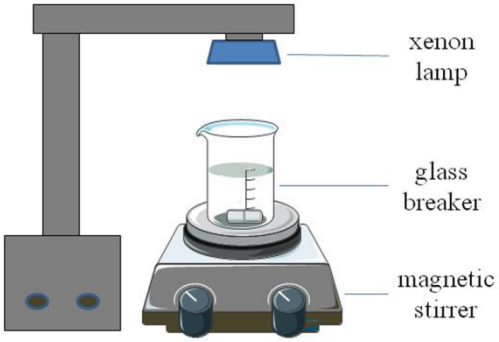

Fig. S-1. Schematic diagram of the photocatalytic reactor.

RSM optimization method

In this work, four parameters were selected as variables, namely initial MB concentration (mg L^{-1}), catalyst dosage (g L^{-1}), solution pH, and reaction time (min), which were labeled as X_1, X_2, X_3, and X_4, respectively. At the same time, the degradation rate of MB dye was used as the output response (Y). The experimental design, mathematical modeling and response optimization were completed by Design Expert 8.0.7.1 software (Stat-Ease, Inc.). For statistical calculation, the variable X_i was encoded as x_i according to the equation (S1):

$$x_i = \frac{X_i - X_0}{\delta X} \quad \text{(S-1)}$$

Where, x_i is the coded value, X_i is the uncoded value, X_0 is the center point value of X_i, and δX represents the step size. In addition, a second-order regression model was used to determine and analyze the response of independent variables. The formula is shown in Equation (S2):

$$Y = \beta_0 + \sum_{i=1}^{k} \beta_i X_i + \sum_{i=1}^{k} \beta_{ii} X_i^2 + \sum_i \sum_j \beta_{ij} X_i X_j \quad \text{(S-2)}$$

Where, Y is the response value (MB degradation rate), X_i and X_j are the variables that affect the response value, β_i is the first-order regression coefficient, β_{ii} is the second-order regression coefficient, and β_{ij} is the interaction coefficient of two independent variables. Finally, the significance and correlation coefficient of the mathematical model were determined by analysis of variance (ANOVA). The quality and predictive reliability of the polynomial were determined by the correlation coefficient (R^2). The range and level of independent variables for MB photodegradation over S-doped g-C_3N_4 are shown in Table S-I.

TABLE S-I. Variables and their codes with corresponding real experimental values

Variables	Coded levels				
	-2	-1	0	1	2
X_1 (mg L^{-1})	3	9	15	21	27
X_2 (g L^{-1})	1	2	3	4	5
X_3	3	5	7	9	11
X_4 (min)	30	60	90	120	150

Economic calculation method

(1) Cost calculation of raw materials

The cost of raw materials mainly included the preparation cost of S-doped g-C_3N_4 and the consumption cost of acid-alkaline regulating reagents, which were the core component of the fixed cost of the photocatalytic process over S-doped g-C_3N_4.

The unit preparation cost of S-doped g-C_3N_4 included raw material procurement, energy consumption, and equipment depreciation, and was determined to be 80 CNY kg^{-1}. The preparation cost for treating 1 m^3 of MB dye wastewater was calculated as follows: Catalyst cost = catalyst mass (kg)×80 CNY kg^{-1}.

The pH adjustment required sodium hydroxide (or hydrochloric acid), with an industrial cost of approximately 2.5 CNY kg^{-1}. The acid/alkali reagent cost for treating 1 m^3 of MB dye wastewater was calculated as follows: acid/alkali reagent cost=acid/alkali reagent dosage (kg)×2.5 CNY kg^{-1}.

(2) Cost calculation of operation

The operating costs mainly included energy consumption (irradiation and stirring) and labor costs. As the main variable-cost component, operating cost depended directly on the reaction time and treatment scale.

Energy consumption in this photocatalytic process primarily arose from the light source and the stirrer. A 300 W xenon lamp was used for irradiation, with an electricity tariff of 0.6 CNY kWh^{-1}, and stirring was provided by a 50 W mixer. As the energy consumption increased with reaction time, the energy-consumption cost for treating 1 m^3 of methylene blue wastewater was calculated as: energy cost=[light source power (kW)+stirrer power (kW)]×reaction time (h)×0.6 CNY kWh^{-1}.

The labor cost mainly included wastewater monitoring, parameter adjustment, equipment maintenance, and other labor costs. The per capita wage of industrial production was set as 6,000 CNY $month^{-1}$, equivalent to 30 CNY $hour^{-1}$. Assuming that the operation time was positively correlated with the reaction time, the labor cost for treating 1 m^3 MB dye wastewater was calculated as follows: labor cost=reaction time (h)×30 CNY h^{-1}.

(3) Integrated cost calculation

Combined with raw material cost and operation cost, the integrated cost for treating 1 m^3 MB dye wastewater could be calculated as follows: integrated cost=(raw material cost + operation cost)=(catalyst cost + acid/alkali reagent cost + energy cost + labor cost).

RESULTS AND DISCUSSION

TABLE S-II. Experimental matrix designed by CDD and experimental and predicted values of Y response

runs	X_1	X_2	X_3	X_4	Y (%)	
					experimental	predicted
1	0.000	0.000	0.000	0.000	66.78	66.39
2	-1.000	-1.000	1.000	1.000	62.91	61.26
3	0.000	0.000	0.000	0.000	66.24	66.39
4	2.000	0.000	0.000	0.000	63.4	60.13
5	-1.000	1.000	-1.000	-1.000	11.02	5.64
6	0.000	2.000	0.000	0.000	16.78	17.38
7	-1.000	1.000	-1.000	1.000	31.93	31.90
8	-2.000	0.000	0.000	0.000	40.84	42.36
9	-1.000	1.000	1.000	1.000	60.29	60.22
10	1.000	1.000	-1.000	1.000	34.64	38.95
11	1.000	-1.000	1.000	1.000	98.72	95.11
12	0.000	0.000	0.000	-2.000	21.47	23.43
13	0.000	0.000	0.000	2.000	81.74	79.24
14	1.000	-1.000	-1.000	1.000	73.5	69.18
15	-1.000	-1.000	-1.000	1.000	58.38	59.48
16	0.000	-2.000	0.000	0.000	76.11	75.89
17	0.000	0.000	0.000	0.000	66.27	63.18
18	0.000	0.000	-2.000	0.000	25.59	25.78
19	0.000	0.000	2.000	0.000	16.76	16.49
20	0.000	0.000	0.000	0.000	66.17	66.36
21	0.000	0.000	0.000	0.000	66.87	66.36
22	1.000	1.000	-1.000	-1.000	16.53	16.59
23	-1.000	1.000	1.000	-1.000	31.56	32.13
24	0.000	0.000	0.000	0.000	66.43	66.36
25	-1.000	-1.000	1.000	-1.000	62.88	61.86
26	-1.000	-1.000	-1.000	-1.000	29.54	29.13
27	1.000	-1.000	1.000	-1.000	70.79	71.00
28	1.000	-1.000	-1.000	-1.000	39.89	40.16
29	1.000	1.000	1.000	1.000	67.48	67.16
30	1.000	1.000	1.000	-1.000	41.42	41.10

507 Table S-III. ANOVA analysis for second-order polynomial regression.

Source	Sum of squares	Degree of freedom	Mean square	F value	p value (Prob > F)	
model	13659.70	14	975.69	8.09	0.0001	significant
X_1	811.77	1	811.77	6.73	0.0204	
X_2	4277.34	1	4277.34	35.45	< 0.0001	
X_3	1394.77	1	1394.77	11.56	0.0040	
X_4	3869.94	1	3869.94	32.07	< 0.0001	
X_1X_2	120.56	1	120.56	1.00	0.3334	
X_1X_3	45.83	1	45.83	0.38	0.5469	
X_1X_4	46.24	1	46.24	0.38	0.5452	
X_2X_3	9.99	1	9.99	0.083	0.7775	
X_2X_4	0.72	1	0.72	0.006	0.9393	
X_3X_4	21.90	1	21.90	0.18	0.6761	
X_1^2	168.67	1	168.67	1.40	0.2555	
X_2^2	416.88	1	416.88	3.45	0.0828	
X_3^2	2862.65	1	2862.65	23.72	0.0002	
X_4^2	186.64	1	186.64	1.55	0.2327	
resudiul	1810.03	15	120.67			
R^2	0.9588					
ajusted R^2	0.9189					

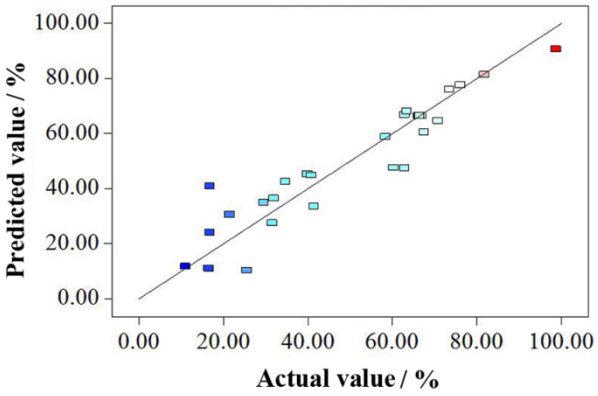

508
509 Fig. S-2. The plots of predicted values versus actual values.

510

Table S-IV. Comparative analysis data of raw material cost for treating 1 m^3 MB wastewater before and after optimization.

	catalyst cost data		acid-alkaline cost data		net saving (CNY)
	dosage (kg)	cost (CNY)	dosage (kg)	cost (CNY)	
before optimization	5	400	0	0	
after optimization	4.1	328	0.12	0.3	71.7
saving cost	—	72	—	-0.3	

Table S-V. Comparative analysis data of operation cost for treating 1 m^3 MB wastewater before and after optimization.

	energy cost data		labor cost data		net saving (CNY)
	energy consumption (kWh)	cost (CNY)	operation time (h)	cost (CNY)	
before optimization	1.050	0.630	3.5	105	
after optimization	0.742	0.445	2.5	75	30.185
saving cost	—	0.185	—	30	